SIGNAL MODEL BASED APPROACH TO JOINT JITTER AND NOISE DECOMPOSITION

White paper | Version 01.00 | Adrian Ispas, Julian Leyh, Andreas Maier, Bernhard Nitsch

ROHDE & SCHWARZ

Make ideas real

ABSTRACT

We propose a joint jitter and noise analysis framework for serial PAM transmission based on a parametric signal model. Our approach has several benefits over state-of-the-art methods. First, we provide additional measurements. Second, we require shorter signal lengths for the same accuracy. Finally, our method does not rely on specific symbol sequences. In this paper, we show example measurement results as well as comparisons with state-of-the-art methods.

AUTHORS BIOGRAPHY

Adrian Ispas received Dipl.-Ing. and Dr.-Ing. degrees in Electrical Engineering and Information Technology from RWTH Aachen University, Aachen, Germany, in 2007 and 2013, respectively. Since 2013, he has been with Rohde & Schwarz GmbH & Co. KG, Munich, Germany, where he is now a Senior Development Engineer in the Center of Competence for Signal Processing.

Julian Leyh obtained his M.Sc. degree in the field of Electrical Engineering from TU Munich in 2017 specializing in communications engineering. He then began his professional career as a member of the Center of Competence for Signal Processing at Rohde & Schwarz. His current focus is on time domain high-speed digital signal analysis.

Andreas Maier received an M.S. degree in Electrical Engineering and Ph.D. degree from the Karlsruhe Institute of Technology (KIT), Germany in 2005 and 2011, respectively. In 2011, he joined Rohde & Schwarz, Munich, Germany. His areas of expertise are digital signal processing and signal integrity. He is a lecturer at the Baden-Wuerttemberg Cooperative State University Stuttgart, Germany.

Bernhard Nitsch is the director of the Center of Competence of Signal Processing at Rohde & Schwarz in Munich, Germany. He and his team focus on signal processing algorithms and systems in the area of signal analysis, spectral analysis, power measurement, security scanners and oscilloscopes. Rohde & Schwarz products contain software, FPGA or ASIC based signal processing components developed in the Center of Competence. He joined Rohde & Schwarz in 2000 and holds a PhD degree in Electrical Engineering and Information Technology from Darmstadt University of Technology, Germany and an M.S. degree in Electrical Engineering from Aachen University of Technology, Germany. He is author of one book and seven technical papers and holds more than 25 patents.

ACKNOWLEDGEMENT

CONTENTS

1   INTRODUCTION

The identification of jitter and noise sources is critical when debugging failure sources in the transmission of high-speed serial signals. With ever increasing data rates accompanied by decreasing jitter budgets and noise margins, managing jitter and noise sources is of utmost relevance. Methods for decomposing jitter have matured considerably over the past 20 years; however, they are mostly based on time interval error (TIE) measurements alone [1, 2]. This TIE-centric view discards a significant portion of the information present in the input signal and thus limits the decomposition accuracy.

The field of jitter separation was conceived in 1999 by M. Li et al. with the introduction of the Dual-Dirac method [3]. The Dual-Dirac method was augmented and improved over the next two decades. Originally, it was meant to isolate deterministic from random jitter components based on the probability density of the input signal's TIEs. It uses the fact that deterministic and random jitter are statistically independent and that deterministic jitter is bounded in amplitude, while random jitter is generally unbounded. Three years later, M. Li et al. reported that their Dual-Dirac method systematically overestimates the deterministic component [4]. Despite this flaw, modelling jitter using the Dual-Dirac model has maintained significance in commercial jitter measurement solutions due to its simplicity [5].

Throughout the years, additional techniques were added to the original Dual-Dirac method to separate additional jitter sources such as intersymbol interference (ISI), periodic jitter (PJ) and other bounded uncorrelated (OBU) jitter. For example, PJ components can be extracted using the autocorrelation function [6] or the power spectral density [7, 8] of the TIEs, while the ISI part of deterministic jitter can be determined by averaging periodically repeating or otherwise equal signal segments [13]. Yet another method for estimating ISI makes use of the property that ISI can be approximately described as a superposition of the effect of individual symbol transitions on their respective TIE [12]. Once the probability density function of one jitter component is known, any second component can be estimated from a mix of the two by means of deconvolution approaches, as long as the components are statistically independent of each other [9, 10, 11].

Collectively, over 40 IEEE publications and more than 50 patents can be found on the topic of jitter analysis alone. Despite this, applications in industrial jitter measurements commonly use a combination of the previously described methods [14, 15, 16], all based solely on TIEs.

In this paper, we first introduce a parametric signal model for serial pulse-amplitude modulated (PAM) transmission that includes jitter and noise contributions. The key to this model is a set of step responses, which characterizes the deterministic behavior of the transmission system, similar to the impulse response in traditional communication systems. Based on the signal model, we propose a joint jitter and noise analysis framework that takes into account all information present in the input signal. This framework relies on a joint estimation of model parameters, from which we readily obtain the commonly known jitter and noise components. Therefore, we provide a single mathematical base yielding the well-known jitter/noise analysis results for PAM signals and thus a consistent impairment analysis for high-speed serial transmission systems.

Additionally, we provide deep system insight through the introduction of new measurements, such as what-if signal reconstructions based on a subset of the underlying impairments. These reconstructions enable the visualization of eye diagrams for a selection of jitter/noise components, thereby allowing informed decisions about the relevance of the selected components. Similarly, we determine selective symbol error rate (SER) and bit error rate (BER) extrapolations to allow fast calculation of (selective) peak-to-peak jitter and noise amplitudes at low error rates.

The proposed framework is inherently able to perform accurate measurements even using relatively short input signals. This is due to the significant increase in information extracted from the signal. Furthermore, our approach has no requirements regarding specific input symbol sequences, such as predefined compliance patterns. On the contrary, the random or scrambled input data typically encountered in real-world scenarios is ideally suited to the framework.

2 SIGNAL MODEL

The proposed joint jitter and noise analysis framework is based on a signal model for serial PAM data transmission. This model assumes the total signal, i.e. the received signal containing all components, to be

$$y(t) = \sum_{k=-\infty}^{\infty} \Delta_s[k] \cdot h_{\mathrm{sr}}(t - T_{\mathrm{clk}}[k] - \epsilon_h[k], \mathbf{s}) + y_{-\infty} + \epsilon_v(t) \tag{1}$$

Here, $\mathbf{s}$ denotes the vector of the transmitted PAM symbol sequence $\{s[k]\}_{k=-\infty}^{\infty}$ and $\Delta_s[k] = s[k] - s[k-1]$ the symbol difference at symbol index k. $h_{\mathrm{sr}}(t, \mathbf{s})$ denotes the step response for the symbol vector $\mathbf{s}$ at time t, $T_{\mathrm{clk}}[k]$ the reference clock time at symbol index k, and $y_{-\infty}$ the initial signal value. The disturbance sources are split into horizontal (time) and vertical (signal level) parts: $\epsilon_h[k]$ is the total horizontal source disturbance and $\epsilon_v(t)$ is the total vertical source disturbance. Contrary to traditional communication systems, we use a step response instead of an impulse response to model the total signal. This is due to the fact that an impulse response is neither able to ensure signal continuity under nonlinear (in the signal level domain) horizontal disturbances nor able to reproduce symbol transition asymmetries. The step response includes transmitter, channel and possibly receiver effects, all of which result in a data-dependent signal disturbance, i.e. intersymbol interference. Moreover, the step response depends on the symbol vector $\mathbf{s}$ in order to account for effects like symbol transition dependencies in the transmission system. In the following, we assume the step response to depend only on the last symbol and the last symbol transition:

$$h_{\mathrm{sr}}(t - T_{\mathrm{clk}}[k] - \epsilon_h[k], \mathbf{s}) = h_{\mathrm{sr}}(t - T_{\mathrm{clk}}[k] - \epsilon_h[k], \{s[k], \Delta_s[k]\}) \tag{2}$$

We thus have up to $N_{\mathrm{PAM}} \cdot (N_{\mathrm{PAM}} - 1)$ step responses for a signal of PAM order N_{PAM}. The total horizontal and vertical source disturbances $\epsilon_{\mathrm{h}}[k]$ and $\epsilon_{\mathrm{v}}(t)$, respectively, are further decomposed as

$$\epsilon_h[k] = \epsilon_{h,P}[k] + \epsilon_{h,\mathrm{OBU}}[k] + \epsilon_{h,R}[k] = \sum_{l=0}^{N_{P(h)}-1} A_{h,l} \sin(2\pi f_{h,l} T_{h,l}[k] + \phi_{h,l}) + \epsilon_{h,\mathrm{OBU}}[k] + \epsilon_{h,R}[k]$$

$$\epsilon_v(t) = \epsilon_{v,P}(t) + \epsilon_{v,\mathrm{OBU}}(t) + \epsilon_{v,R}(t) = \sum_{l=0}^{N_{P(v)}-1} A_{v,l} \sin(2\pi f_{v,l} t + \phi_{v,l}) + \epsilon_{v,\mathrm{OBU}}(t) + \epsilon_{v,R}(t) \tag{3}$$

The horizontal and vertical periodic components $\epsilon_{h,P}[k]$ and $\epsilon_{v,P}(t)$, respectively, are characterized by the amplitudes $A_{x,l}$, the frequencies $f_{x,l}$ and the phases $\phi_{x,l}$ for $l = 0, \dots, N_{P(x)} - 1$ and $x = \{h,v\}$, respectively, and $T_{h,l}[k]$ denotes the relevant point in time for the horizontal periodic component l at symbol k. The terms $\epsilon_{h,\text{OBU}}[k]$ and $\epsilon_{v,\text{OBU}}(t)$ designate other bounded uncorrelated (OBU)[1] components, and the random components $\epsilon_{h,R}[k]$ and $\epsilon_{v,R}(t)$ denote additive noise for the horizontal and vertical case, respectively. At this point, we do not impose any statistical properties on the random components.

3   JITTER AND NOISE DECOMPOSITION

As introduced in section 2, various effects cause disturbances in transmitted data. The transmitter and the channel have the most influence on the step responses that determine the data-dependent disturbance of the signal (intersymbol interference). Periodic and OBU disturbances make up the remaining deterministic and bounded components. Finally, there are random and unbounded disturbances such as thermal noise. Apart from being deterministic and bounded, very little information is available about OBU components at the receiver end. Therefore, we omit OBU components from now on. Their influence will be visible in the extracted random components.

3.1   Source and analysis domains

With the exception of data-dependent components, all disturbances are either of horizontal or vertical origin. The horizontal components constituting $\epsilon_h[k]$ originate at the transmitter, whereas the vertical components in $\epsilon_v(t)$ may also be added in the channel or at the receiver end. The data-dependent components have their origin in the combination of the data, i.e. the transmitted symbols, and the step responses that overlap to build the signal. We thus define the *source domain* to be either "horizontal", "vertical" or "data".

Analyzing the disturbances in the time domain is referred to as jitter analysis. Timing errors with respect to a reference clock signal are determined and analyzed. This is usually done by means of the TIE. However, the disturbances can also be analyzed in the signal level domain, which is referred to as noise analysis. In this case, signal level errors with respect to reference levels are determined and analyzed at symbol sampling times given by a reference clock signal. Fig. 1 depicts the definition of the TIE and the level error (LE). The choice between jitter analysis and noise analysis is a choice of the *analysis domain*, which we accordingly define to be either "jitter" or "noise".

Fig. 1: TIE and LE definition

---
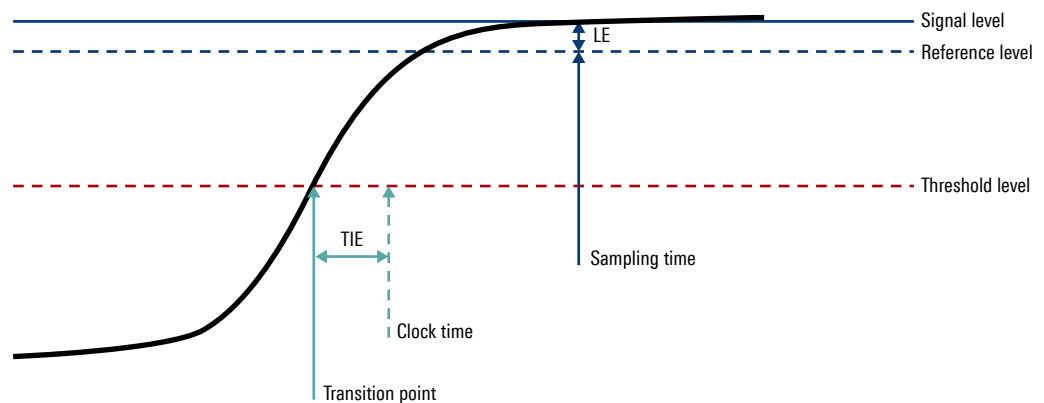
[1]   The word "other" in OBU refers to the nonperiodicity of the disturbance and the word "uncorrelated" to the nonexistence of any correlation between the disturbance and the symbol sequence.

3.2 Decomposition tree

The decomposition tree of total jitter and total noise is depicted in Fig. 2. It is important to remember that, as shown in Fig. 2, horizontal disturbances also have an influence in the noise domain and vertical disturbances in the jitter domain. Thus no matter whether a jitter or a noise analysis is performed, all disturbance components need to be accounted for, i.e. for any analysis domain, all source domains are relevant. Moreover, it is generally not possible to directly map properties in a source domain to measurements in an analysis domain. Consider, e.g. the case of the horizontal random source disturbance $\epsilon_{h,R}[k]$ only. Its effect on the signal level and thus the noise domain can be described by a Taylor series of $\epsilon_{h,R}[k]$ around the mean. For the zero-mean case, we obtain

$$y_{R(h)}(t) = \sum_{n=1}^{\infty} \frac{1}{n!} \sum_{k=-\infty}^{\infty} \Delta_s[k] \cdot \frac{\partial^n}{\partial t^n} h_{\mathrm{sr}}(t - T_{\mathrm{clk}}[k], \{s[k], \Delta_s[k]\}) \cdot (-\epsilon_{h,R}[k])^n \quad (4)$$
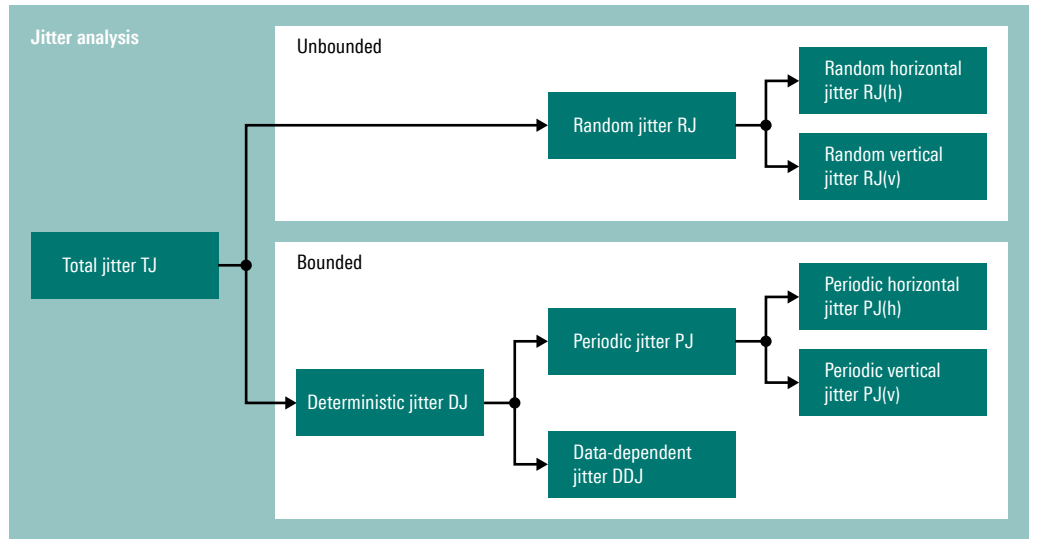
The first-order approximation of equation (4) is given by

$$\tilde{y}_{R(h)}(t) = -\sum_{k=-\infty}^{\infty} \Delta_s[k] \cdot \frac{\partial}{\partial t} h_{\mathrm{sr}}(t - T_{\mathrm{clk}}[k], \{s[k], \Delta_s[k]\}) \cdot \epsilon_{h,R}[k] \quad (5)$$

We recognize that the horizontal random source disturbances are transformed to the noise domain in a nonlinear manner that depends on the step responses and their derivatives[2]. Moreover, the inverse step of determining the source disturbance based on the noise disturbance is nontrivial.

Fig. 2: Jitter and noise decomposition tree
a) Jitter analysis

---

[2] For jointly stationary $\epsilon_{h,R}[k]$ and $s[k]$, and $T_{\mathrm{clk}}[k] = kT_s$ with the constant symbol period T_s, the first-order approximation (5) is cyclostationary. Moreover, for PAM signals of order $N_{\mathrm{PAM}} > 2$ and Gaussian distributed $\epsilon_{h,R}[k]$, $\tilde{y}_{R(h)}(t)$ is not Gaussian distributed since the symbol difference $\Delta_s[k]$ can take on values with different amplitudes.
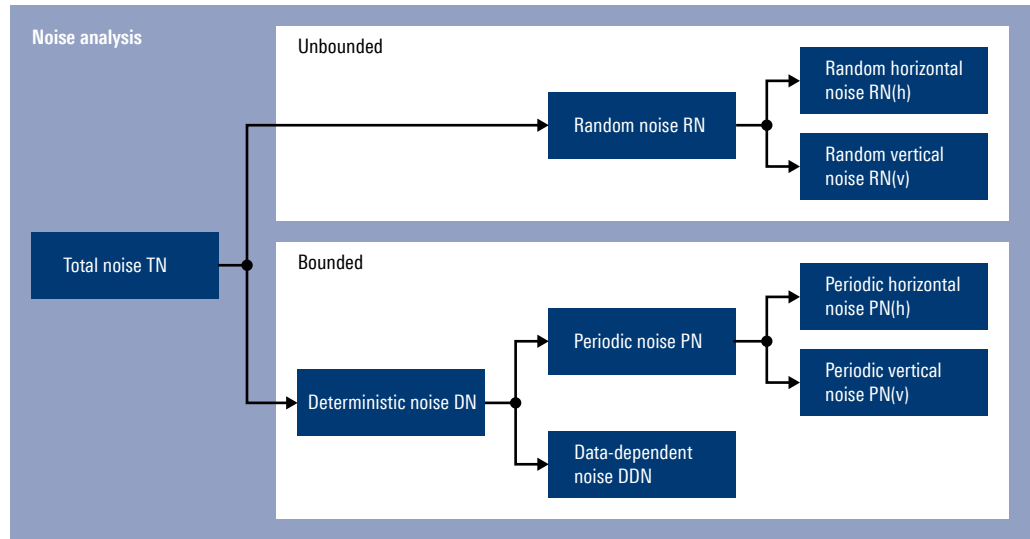
4 JOINT JITTER AND NOISE ANALYSIS FRAMEWORK

We propose a framework that encompasses a joint jitter and noise analysis and is based on the signal model introduced in section 2. Contrary to state-of-the-art methods, which transition from a signal to a TIE representation as a first step, our approach is based directly on the total signal. It thus does not discard any information present in the (total) signal by using a condensed representation like TIEs do. The core of our framework operates independently of the analysis domain (jitter or noise) and considers all source domains (horizontal, vertical and data). The jitter and noise results are derived from a joint set of estimated model parameters.

Conceptually, the first step of the framework is to recover a clock that makes it possible to decode, i.e. recover, the data symbols. Based on the recovered clock signal and the decoded symbols, a joint estimation of model parameters is performed. Specifically, a coarse, partly spectrum based estimator recovers rough estimates of the frequencies and phases of the vertical periodic components as well as their number. These are then used for a fine, least-squares estimator that jointly determines the step responses and the periodic vertical components. The horizontal periodic components are similarly estimated. These estimates, along with the recovered symbols and clock, allow synthesis of signals with only selected disturbance components, e.g. the data-dependent signal. We then use the total and synthesized signals to transition to the analysis domains and calculate jitter and noise values, i.e. TIE and LE values, respectively. Fig. 3 shows a block diagram of the framework.

Fig. 3: Joint jitter and noise analysis framework
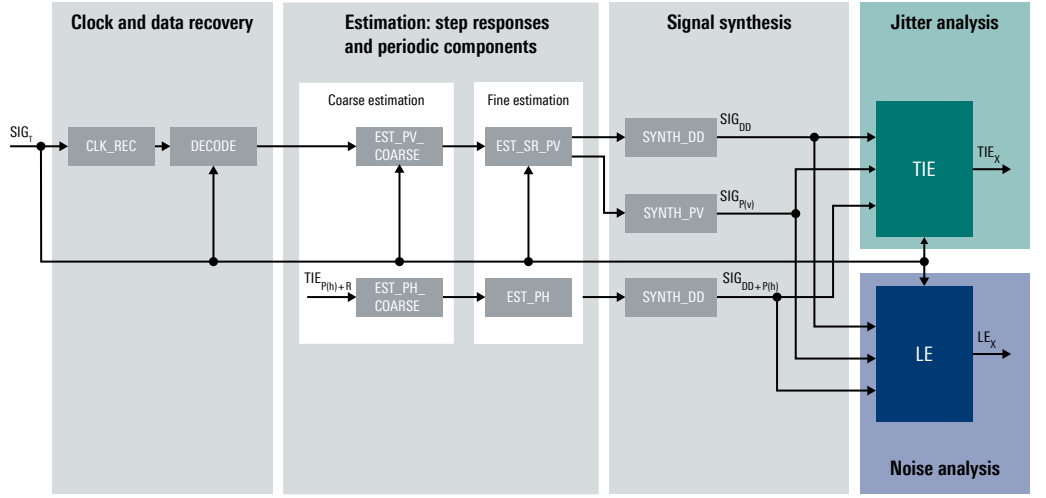
4.1 Estimation of model parameters

The fine estimator that performs a joint estimation of the model parameters is at the core of the framework and is derived as follows. First, we need to treat the remaining horizontal disturbances $\epsilon_{h,\mathrm{rem}}[k]$ as additive noise for the estimator. Their influence in the signal level domain is quantified as in (5) by linearizing (1) with respect to $\epsilon_{h,\mathrm{rem}}[k]$:

$$y_{h,\mathrm{rem}}(t) \approx \tilde{y}_{h,\mathrm{rem}}(t) = -\sum_{k=-\infty}^{\infty} \check{\Delta}_s[k] \cdot h(t - \check{T}_{\mathrm{clk}}[k], \{\check{s}[k], \check{\Delta}_s[k]\}) \cdot \epsilon_{h,\mathrm{rem}}[k] \quad (6)$$

where $\check{s}[k]$ is the decoded symbol, $\check{\Delta}_s[k]$ the corresponding symbol difference, $h(t, \check{s}[k], \check{\Delta}_s[k])$ the impulse response, and $\check{T}_{\mathrm{clk}}[k]$ an estimated clock time.

By further approximating the vertical sinusoidal components, we obtain

$$\epsilon_{v,P}(t) \approx \tilde{y}_{P(v)}(t) = \sum_{l=0}^{N_P(v)-1} A_{v,l}\sin(2\pi \check{f}_{v,l}t + \check{\phi}_{v,l}) + A_{v,l}(\Delta_{f,v,l}2\pi t + \Delta_{\phi,v,l})\cos(2\pi \check{f}_{v,l}t + \check{\phi}_{v,l}) \quad (7)$$

with the frequencies $f_{v,l} = \check{f}_{v,l} + \Delta_{f,v,l}$ and the phases $\phi_{v,l} = \check{\phi}_{v,l} + \Delta_{\phi,v,l}$ split into coarse and remaining parts for $l = 0, \ldots, N_{P(v)} - 1$. This yields the following approximation of the total signal:

$$y(t) \approx \tilde{y}(t) = \sum_{k=-\infty}^{\infty} \check{\Delta}_s[k] \cdot h_{\mathrm{sr}}(t - \check{T}_{\mathrm{clk}}[k], \{\check{s}[k], \check{\Delta}_s[k]\}) + y_{-\infty} + \tilde{y}_{P(v)}(t) + \epsilon_{v,R}(t) + \tilde{y}_{h,\mathrm{rem}}(t) \quad (8)$$

The coarse estimates and the above approximations can be used to perform a (fine) joint least-squares estimation of the step responses and the vertical periodic components:

$$\hat{\mathbf{x}} = \begin{bmatrix} \hat{\mathbf{h}}_{\mathrm{sr}} \\ \hat{y}_{-\infty} \\ \hat{\mathbf{p}} \end{bmatrix} = \mathbf{A}^{+}\mathbf{y} \quad (9)$$

with the estimate vector $\hat{\mathbf{x}}$ containing the N_{sr} estimates of the step responses in the vector $\hat{\mathbf{h}}_{\mathrm{sr}}$, the initial signal value estimate $\hat{y}_{-\infty}$, and the estimates of the frequencies, phases, and amplitudes of the vertical periodic components in the vector $\hat{\mathbf{p}}$.

The matrix $\mathbf{A}^+$ is the pseudoinverse of the observation matrix and the vector $\mathbf{y}$ contains samples of the total signal. Based on these estimates and the recovered (or input) clock signal $T_{\mathrm{cdr}}[k]$, the data-dependent (DD) and the periodic vertical ($P(v)$) signals can be synthesized as

$$\hat{y}_{DD}(t) = \sum_{k=-\infty}^{\infty} \check{\Delta}_s[k] \cdot \hat{h}_{\mathrm{sr}}(t - T_{\mathrm{cdr}}[k], \check{\Delta}_s[k]) + \hat{y}_{-\infty}$$

$$\hat{y}_{P(v)}(t) = \sum_{l=0}^{N_{P(v)}-1} \hat{A}_{v,l} \sin(2\pi \hat{f}_{v,l} t + \hat{\phi}_{v,l}) \tag{10}$$

The horizontal periodic components are estimated in a two-step approach as above. More precisely, the estimation is based on the time difference

$$T_{\mathrm{sig},T}[k] - T_{\mathrm{sig},DD+P(v)}[k] \tag{11}$$

where $T_{\mathrm{sig},T}[k]$ and $T_{\mathrm{sig},DD+P(v)}[k]$ are the level crossing time of the total and the $DD + P(v)$ signal, respectively. Thus an estimate of the horizontal periodic ($P(h)$) contribution to the level crossing times is obtained and the $DD + P(h)$ signal can be synthesized.

Summarizing, we are able to synthesize signals with a subset of the underlying source disturbances. These what-if signal reconstructions allow us to provide new measurements with selectable disturbances. For example, it is possible to construct an eye diagram with data disturbances and chosen periodic disturbances only. The measurements carried out in the analysis domains are described in the following sections.

4.2 Analysis domains

Based on the total and the synthesized signals, we move away from a signal-centric view in order to obtain the commonly known jitter/noise values. Specifically, we determine TIEs defined as

$$\mathrm{TIE}_X[k] = T_{\mathrm{sig},X}[k] - T_{\mathrm{cdr}}[k] \tag{12}$$

where $T_{\mathrm{sig},X}[k]$ is the level crossing time of the signal $X = \{DD, DD+P(h), DD+P(v), D, T\}$. For the remaining TIEs, we impose the following relationships:

$$\begin{aligned}
\mathrm{TIE}_T[k] &= \mathrm{TIE}_D[k] + \mathrm{TIE}_R[k] \\
\mathrm{TIE}_{DD+P(h)}[k] &= \mathrm{TIE}_{DD}[k] + \mathrm{TIE}_{P(h)}[k] \\
\mathrm{TIE}_{DD+P(v)}[k] &= \mathrm{TIE}_{DD}[k] + \mathrm{TIE}_{P(v)}[k] \\
\mathrm{TIE}_D[k] &= \mathrm{TIE}_{DD}[k] + \mathrm{TIE}_P[k]
\end{aligned} \tag{13}$$

Similarly, for the noise analysis, we determine LEs that are defined with respect to reference signal levels:

$$\mathrm{LE}_X[k] = V_X[k] - V_{\mathrm{ref}}[k] \tag{14}$$

where $V_X[k]$ is the signal value obtained at the symbol sampling times for the signal $X = \{DD, DD+P(h), DD+P(v), D, T\}$ and $V_{\mathrm{ref}}[k]$ is the reference value that depends on the current symbol value.

The remaining LEs are decomposed as in the TIE case, i.e. we use

$$\mathrm{LE}_T[k] = \mathrm{LE}_D[k] + \mathrm{LE}_R[k] \tag{15}$$

and thus the remaining LEs can be computed.

5 MEASUREMENTS

Various measurements of interest can be obtained based on the TIEs and the LEs introduced in yection 4.2. The TIE statistics can either be computed for all values or for specific subsets, e.g. rising or falling edges. Similarly, the LE statistics can be computed for certain symbol values only. The measurements are briefly presented in the following subsections.

5.1 Statistical values and histograms

We calculate common statistical values like the minimum, maximum, peak-to-peak value, power and standard deviation (SD) for both the TIEs and the LEs. Furthermore, we use histogram plots to illustrate the shape of their distribution.

5.2 Duty cycle distortion and level distortion

In the context of a jitter analysis, the duty cycle distortion (DCD) is calculated as

$$\mathrm{DCD} = \max_{k=0,\ldots,N_{\mathrm{sr}}-1} \{\mathrm{E}\{\mathrm{TIE}_{DD}|h_{\mathrm{sr},k}\}\} - \min_{k=0,\ldots,N_{\mathrm{sr}}-1} \{\mathrm{E}\{\mathrm{TIE}_{DD}|h_{\mathrm{sr},k}\}\} \tag{16}$$

where $\mathrm{E}\{x\}$ denotes the expectation of the random variable x and $h_{\mathrm{sr},k}$ the occurrence of the k-th step response with $k = 0, \ldots, N_{\mathrm{sr}} - 1$. The DCD value measures the impact of two effects. First, the differences in the various step responses, e.g. rising and falling step responses in the case of non-return-to-zero (NRZ) signals ($N_{\mathrm{PAM}} = 2$), and second, a mismatch in the signal level thresholds used for determining the TIEs.

The level distortion (LD) for the eye opening l

$$\mathrm{LD}[l] = \mathrm{E}\{\mathrm{LE}_{DD}|\mathrm{level} = l + 1|\} - \mathrm{E}\{\mathrm{LE}_{DD}|\mathrm{level} = l\}, \ l = 0, \ldots, N_{\mathrm{PAM}} - 1 \tag{17}$$

is used in the context of noise analysis. It characterizes vertical distortion of the eye opening due to data-dependent disturbances.

5.3 Autocorrelation functions and power spectral densities

Further information can be derived from a spectral view of the TIE and LE tracks. For TIEs, a spectral view is not straightforward to compute since symbol transitions do not occur between every two symbols. Usually, this is handled by linear interpolation between given TIEs. We propose a different approach in order to avoid the introduction of artifacts. First, compute the autocorrelation function of the TIE track by only considering the given TIE values, then compute the power spectral density (PSD) based on the autocorrelation function, thereby obtaining a spectral view without any interpolation artifacts.

5.4 Symbol error rate calculation

SER plots visualize how varying a single parameter affects the number of correctly decoded symbols by plotting the SER against the parameter in question. For a jitter analysis, the SER is plotted against the sampling time offset used to decode the symbols, while for a noise analysis, the parameter is the decision threshold level of the considered eye. Symbol errors occur, e.g. when signal transitions take place after the corresponding symbol has been sampled or signal levels do not cross the threshold level of the desired symbol, respectively. The SER is equivalent to the BER for NRZ signals.

Normally, to measure the SER, the system under test is used to transmit a known symbol sequence and to evaluate the symbol errors in the received signal. Repeating this measurement for a number of values of the desired parameter yields the SER plots. Such a measurement setup usually interferes with the regular operation of the system under test and may therefore be difficult to accomplish or even yield different results. Additionally, SER measurements take a very long time for low SER values like 10^{-12}.

We propose a method to calculate SER plots based on the jitter or noise values, i.e. the TIEs or LEs, respectively, and their statistics. To calculate an SER plot, first select a histogram that covers all desired deterministic components with bins representing the desired analysis domain and a set of probability distribution parameters describing the desired random components in the same analysis domain. For example, when the SER for all signal disturbances plotted against the sampling time offset is desired, we select the TIE histogram covering all deterministic components and the TIE distribution covering all random components. By choosing histograms and distributions that cover only part of the measured signal perturbations, what-if SER plots can be generated that allow the user to gain insight into how the SER would change if the user were to resolve certain signal integrity issues. The information stored in the histogram is, for every bin l_{bin}, the probability of hitting that bin $P_{\text{hist}}[l_{\text{bin}}]$ and the position of that bin $x_{\text{hist}}[l_{\text{bin}}]$. Assuming a probability distribution p_R of the random components, we get the SER

$$\text{SER}(u) = \sum_{l_{\text{bin}}} P_{\text{hist}}[l_{\text{bin}}] \cdot \int_{v \in e(u)} p_R\left(v - x_{\text{hist}}[l_{\text{bin}}]\right) dv \tag{18}$$

where $e(u) = \{x: \text{position } x \text{ generates a decoding error for parameter } u\}$ holds information about the error conditions. Note that while random disturbances are often assumed to be Gaussian distributed, this may not be the case in certain scenarios due to the nonlinear transformation from source to analysis domain (see section 3.2).

5.5 Jitter and noise characterization at a target SER

A number of secondary measurements are derived from the SER calculation. One of these is TJ@SER, the total jitter at a target SER. This value represents the jitter budget that a system designer has to anticipate when trying to reach a target SER. It can be identified as the width of the SER vs. sampling time offset plot at the desired SER.

Another example is the Dual-Dirac value $\text{DJ}_{\delta\delta}$ from the Dual-Dirac model. The Dual-Dirac model assumes that the deterministic jitter can only take on two discrete values and that the relationship

$$\text{TJ@SER} = \text{DJ}_{\delta\delta} + \sigma_{RJ} \cdot c(\text{SER}) \tag{19}$$

holds, where the value $c(\text{SER})$ depends solely on the target SER. Sufficiently low SERs need to be ensured for the above relationship to hold, otherwise the (Gaussian) random jitter does not dominate the total jitter.

For noise analysis, we compute the EH@SER value, which gives the eye height that is achieved at a target SER.

6   FRAMEWORK RESULTS

In this section, we present measurement results from the joint jitter and noise analysis framework presented in section 4. To make the vast amount of measurements and comparisons more accessible, we present a single scenario in section 6.1 and use a majority of the available results to track down a signal integrity issue and understand its implications. In section 6.2, we show how the length of the input signal affects the measurements and thus the framework's performance. The scenarios used in this subsection are summarized in Table 1. We use a second order phase-locked loop (PLL) with a bandwidth factor of 500 and a damping factor of 0.7 for these scenarios.

Table 1: Settings for synthetic scenarios

Property	Scenario 1	Scenario 2
Data rate	5 Gbps	5 Gbps
Sample rate	40 Gsample/s	20 Gsample/s
Number of symbols	300k	variable
Modulation	NRZ, reference levels: −1 and +1	NRZ, reference levels: −1 and +1
Symbol pattern	random	random
Rate modulation	triangular SSC with −5000 ppm at 33 kHz	none
Step response asymmetry	fall time > rise time	none
Periodic horizontal disturbance $\epsilon_{h,P}$	100 mUI pp at 20 MHz	200 mUI pp at 20 MHz
Periodic vertical disturbance $\epsilon_{v,P}$	0.1 pp at 100 MHz	0.02 pp at 20 MHz
Random horizontal disturbance $\epsilon_{h,R}$	20 mUI RMS	50 mUI RMS
Random vertical disturbance $\epsilon_{v,R}$ (SNR)	30 dB	35 dB

6.1   Example analysis

Throughout this section, we use scenario 1 from Table 1, i.e. a synthetic 5 Gbps NRZ data signal with random symbols to show the framework's capabilities.

Fig. 4 shows the data rate over time as recovered by the clock and data recovery (CDR). At the very start of the signal, the CDR's locking behavior can be observed. After the lock time (indicated by the red line), the CDR follows a triangular modulation profile of −5000 ppm at 33 kHz. Such a modulation profile is commonly used for spread spectrum clocking (SSC) in, e.g. USB 3.0. Note that CDR misconfiguration happens quite frequently and is easily caught at this stage.

Fig. 4: Symbol rate from CDR
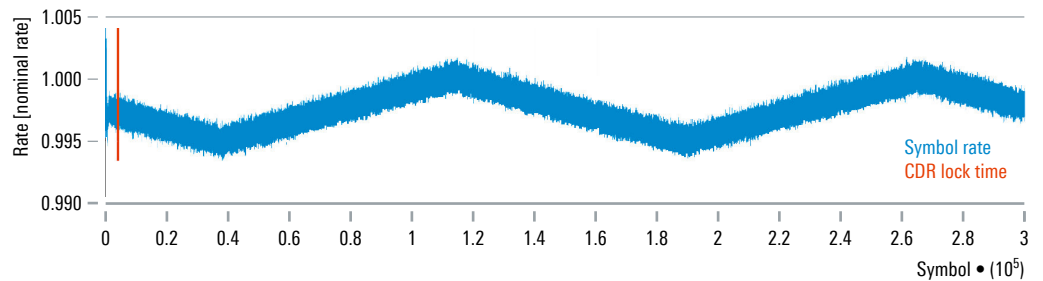
The recovered clock can be used to produce eye diagrams not only of the total signal, but also of synthesized signals covering only a subset of the disturbances in the total signal. This allows the user to graphically assess the most severe causes of signal degradation and to acquire an expectation of what could be achieved in a given scenario once a certain issue is fixed. The variety of available synthetic eye diagrams improves upon the possibilities offered by state-of-the-art methods. Fig. 5 shows some of these eye diagrams: a) the total signal, b) the data-dependent signal, c) the data-dependent signal with periodic horizontal disturbances and d) the signal with all deterministic components. We can see that the data-dependent component is responsible for most of the jitter and noise. Successively adding the periodic disturbances yields signals that approach the jitter and noise of the total signal.

Fig. 5: Total and synthetic eye diagrams

a) T

b) DD

c) DD+P(h)

d) DD+P(h)+P(v)
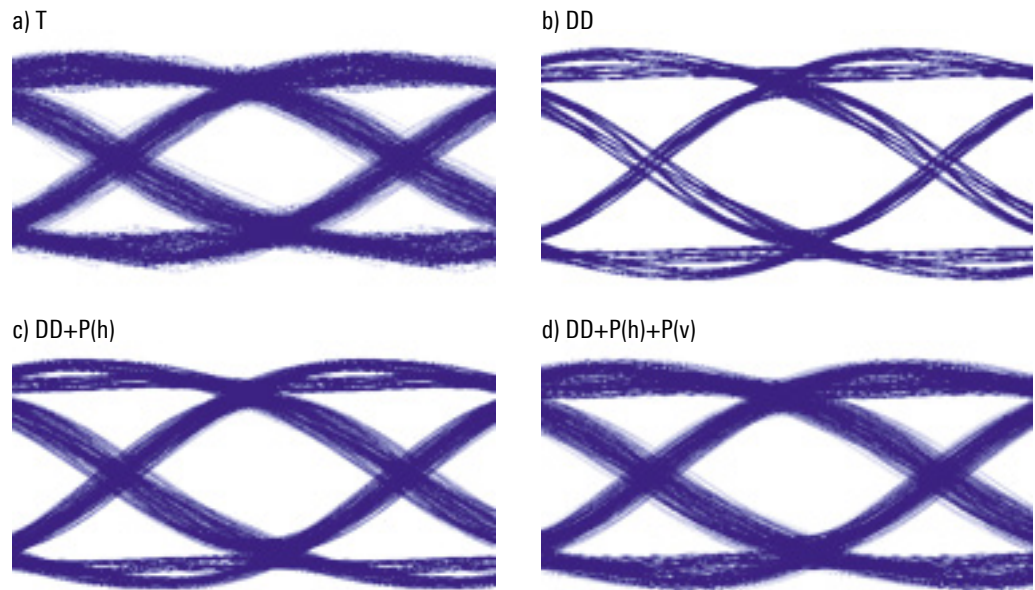
Deeper understanding of the individual jitter and noise components is obtained from TIE and LE histograms as in Fig. 6. These show the distribution of all timing and level errors for various components. Some effects can be seen more easily using TIE histograms for rising and falling edges and LE histograms for symbols 0 and 1. Subplot c) in Fig. 6 shows that falling edges cause significantly more data-dependent jitter than their rising counterparts. Periodic jitter in e) adds a moderate amount of additional jitter. In the noise domain, data-dependent components dominate over periodic components. The random components in g) and h) show a close to Gaussian distribution.

Fig. 6: TIE and LE histograms
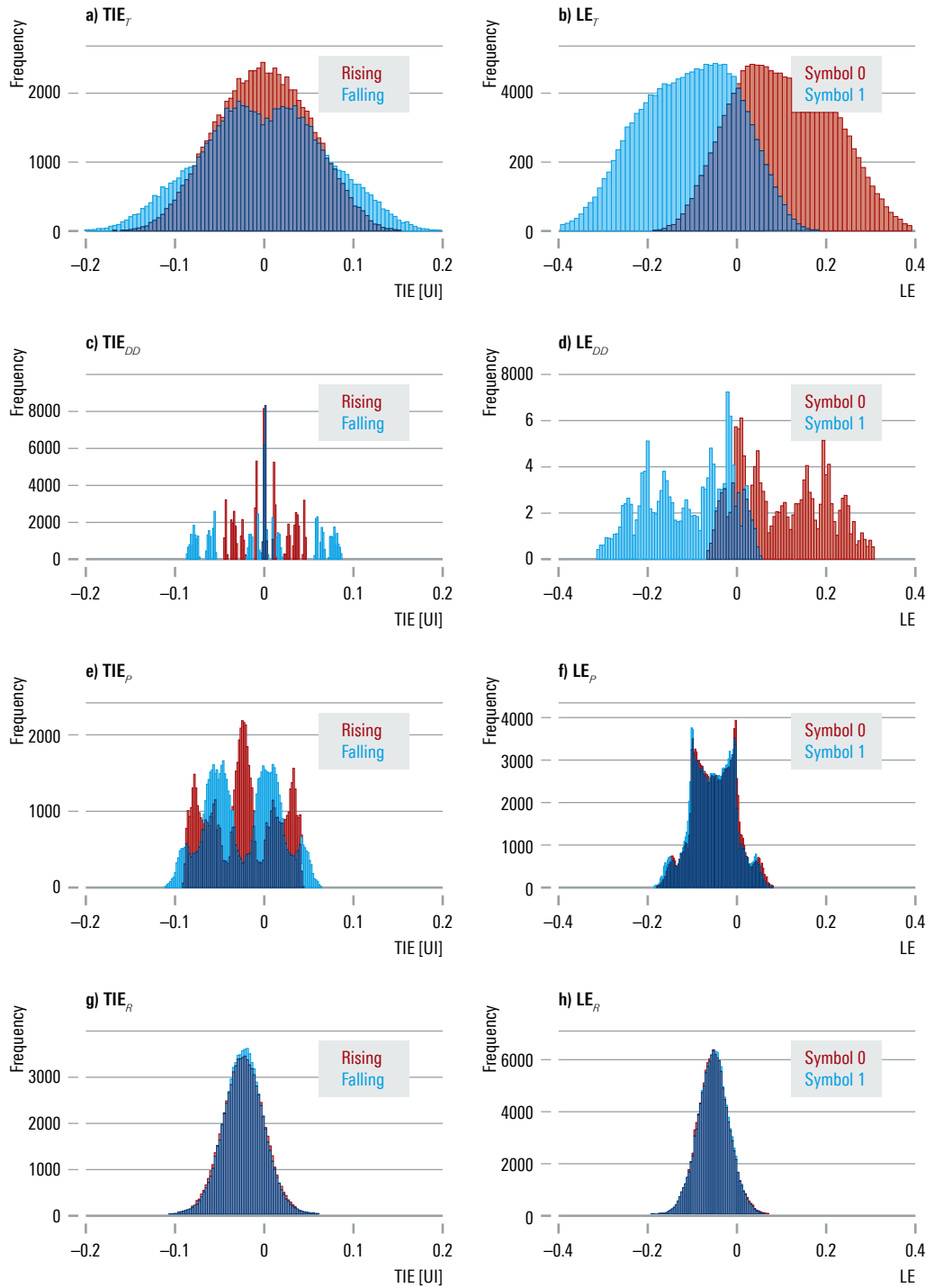
To get a better understanding of the effects shown in the histograms, Table 2 gives some statistical values derived from the TIEs and the LEs. Note that the total and random components have peak-to-peak (PP) values that depend on the signal length.

Table 2: Statistical values of TIEs and LEs

Disturbances	Edges/symbols	TIE [mUI]			LE		
		SD	Mean	PP	SD	Mean	PP
Total	All	60.6	−0.11	448.1	$1.6 \cdot 10^{-1}$	$7.5 \cdot 10^{-5}$	1.06
Total	Rising/0	51.9	−0.12	344.3	$1.1 \cdot 10^{-1}$	$1.1 \cdot 10^{-1}$	0.76
Total	Falling/1	68.2	−0.09	448.1	$1.1 \cdot 10^{-1}$	$-1.1 \cdot 10^{-1}$	0.75
Data-dependent	All	40.0	−0.20	178.1	$1.4 \cdot 10^{-1}$	$5.7 \cdot 10^{-5}$	0.62
Data-dependent	Rising/0	25.7	−0.23	93.0	$9.6 \cdot 10^{-2}$	$1.1 \cdot 10^{-1}$	0.37
Data-dependent	Falling/1	50.4	−0.18	178.1	$9.5 \cdot 10^{-2}$	$-1.1 \cdot 10^{-1}$	0.37
Random	All	22.6	0.17	255.8	$3.5 \cdot 10^{-2}$	$1.7 \cdot 10^{-5}$	0.37
Random	Rising/0	22.8	0.16	202.6	$3.5 \cdot 10^{-2}$	$1.4 \cdot 10^{-4}$	0.34
Random	Falling/1	22.4	0.17	255.8	$3.5 \cdot 10^{-2}$	$-1.1 \cdot 10^{-4}$	0.37

The root cause of the signal integrity issue becomes very clear in Fig. 7, which shows the rising and falling step responses. Clearly, the falling step response shows a much greater fall time than the rise time of its rising counterpart. Such behavior can be triggered by an electrical problem in the transmitter's output stage. Note that the falling step response is flipped to allow a comparison between the two. At this stage, the user has all the information needed to solve the signal integrity issue. The display of step responses is a new feature not offered by state-of-the-art methods.

Fig. 7: Step responses
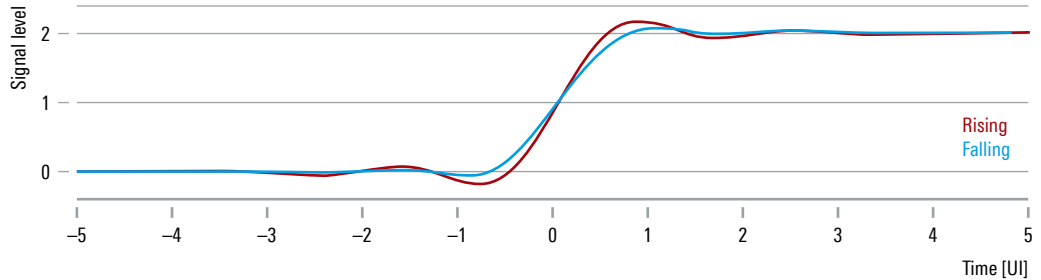
All that remains is to investigate the effects of the issue when left untreated. We provide measured [3] and calculated SERs over sampling time plots. The calculated SER plots are an important result of the overall analysis since they depend on all the previously extracted components and therefore cumulate to a large portion of the results. In Fig. 8 a), we observe that the sampling time window left to obtain a good SER is rather small. In fact, the jitter amounts to more than half of a unit interval (UI) when aiming for an SER of 10^{-12}, a value that is reported as TJ@SER. Analogous to the SER vs. sampling time plot, an SER vs. decision threshold plot is generated from the noise analysis results, see Fig. 8 b). Although the random components in the noise domain are not exactly Gaussian distributed, the SER extrapolation is still accurate at measurable SER values. Note that the measured SERs become unreliable, and thus diverge from the calculated SERs, at low values due to the low number of measured errors.

[3] The SER measurement is based on the assumption that the symbols are correctly decoded at the unit interval center.

Fig. 8: SERs: jitter and noise domain

a) SER vs. sampling time

+ Measured
Calculated T
Calculated $DD + R$

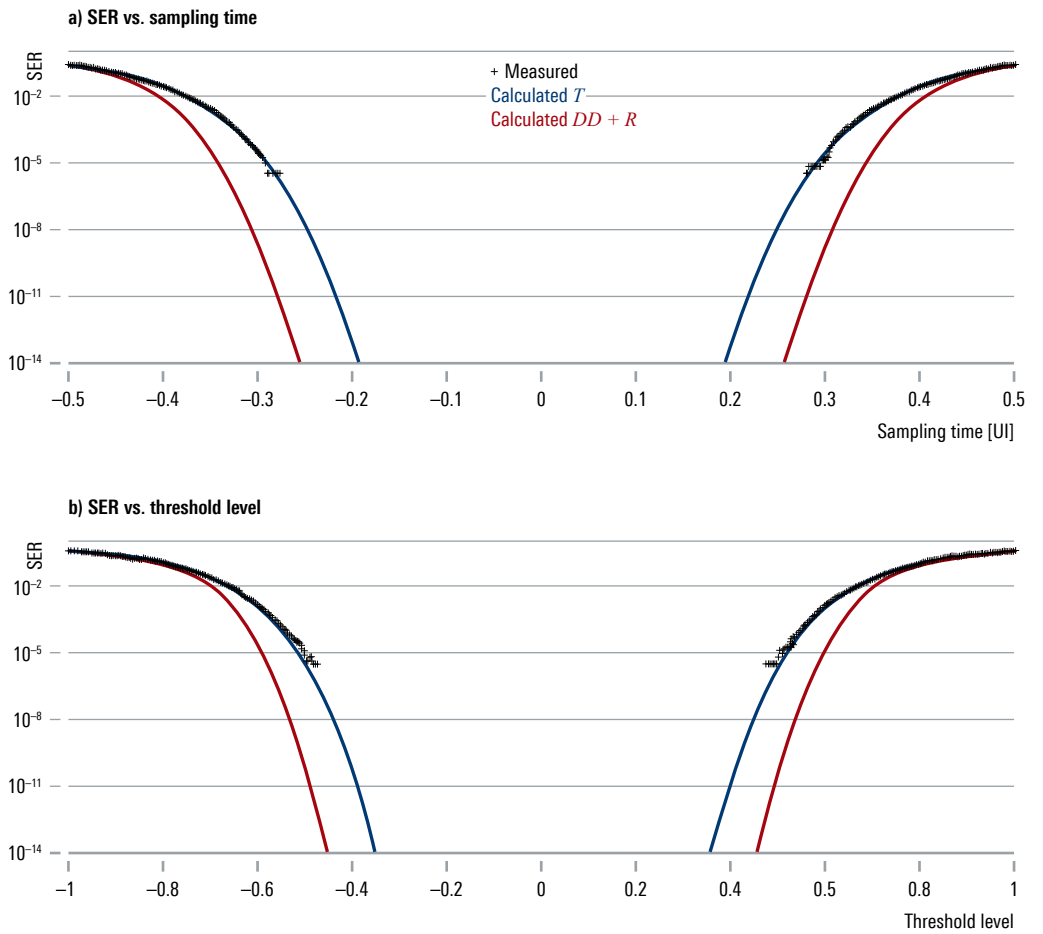**b) SER vs. threshold level**

Table 3 provides the TJ@SER along with the Dual-Dirac and the EH@SER values. It also includes the DCD and LD values, which measure the asymmetry between rising and falling transitions and the symbols 0 and 1, respectively.

### Table 3: Other statistical values

Statistic	Value
DCD	$5.4 \cdot 10^{-1}$ mUI
LD	0.21
TJ@SER = $1 \cdot 10^{-12}$	582.3 mUI
$DD_{\delta\delta}$	263.7 mUI
EH@SER = $1 \cdot 10^{-12}$	0.75

Finally, more information can be derived about the periodic components. Table 4 lists the estimated frequencies and amplitudes of the horizontal and vertical periodic disturbances. Fig. 9 shows TIE and LE PSDs. Compared to state-of-the-art methods, we are able to give PSDs for individual jitter/noise components. The horizontal periodic source disturbance can be identified as peak in the PSD of TIE_T and $TIE_{P(h)}$, while the vertical periodic source disturbance can be identified as peak in the PSD of LE_T and $LE_{P(v)}$. Additionally, the PSD of $TIE_{P(v)}$ shows a peak for the vertical periodic source disturbance since, in this case, we compensate for the sign variation of the TIEs due to the rising and falling step response.

Table 4: Periodic disturbances

Horizontal	Vertical
97 mUI pp at 20.0 MHz	0.100 pp at 100.0 MHz
9.1 mUI pp at 33.4 kHz	$6.5 \cdot 10^{-4}$ pp at 279.4 MHz
3.0 mUI pp at 98.9 kHz	$2.1 \cdot 10^{-4}$ pp at 99.9 MHz
1.6 mUI pp at 165.1 kHz	$1.8 \cdot 10^{-4}$ pp at 100.1 MHz

## Fig. 9: PSDs

a) TIE

b) LE
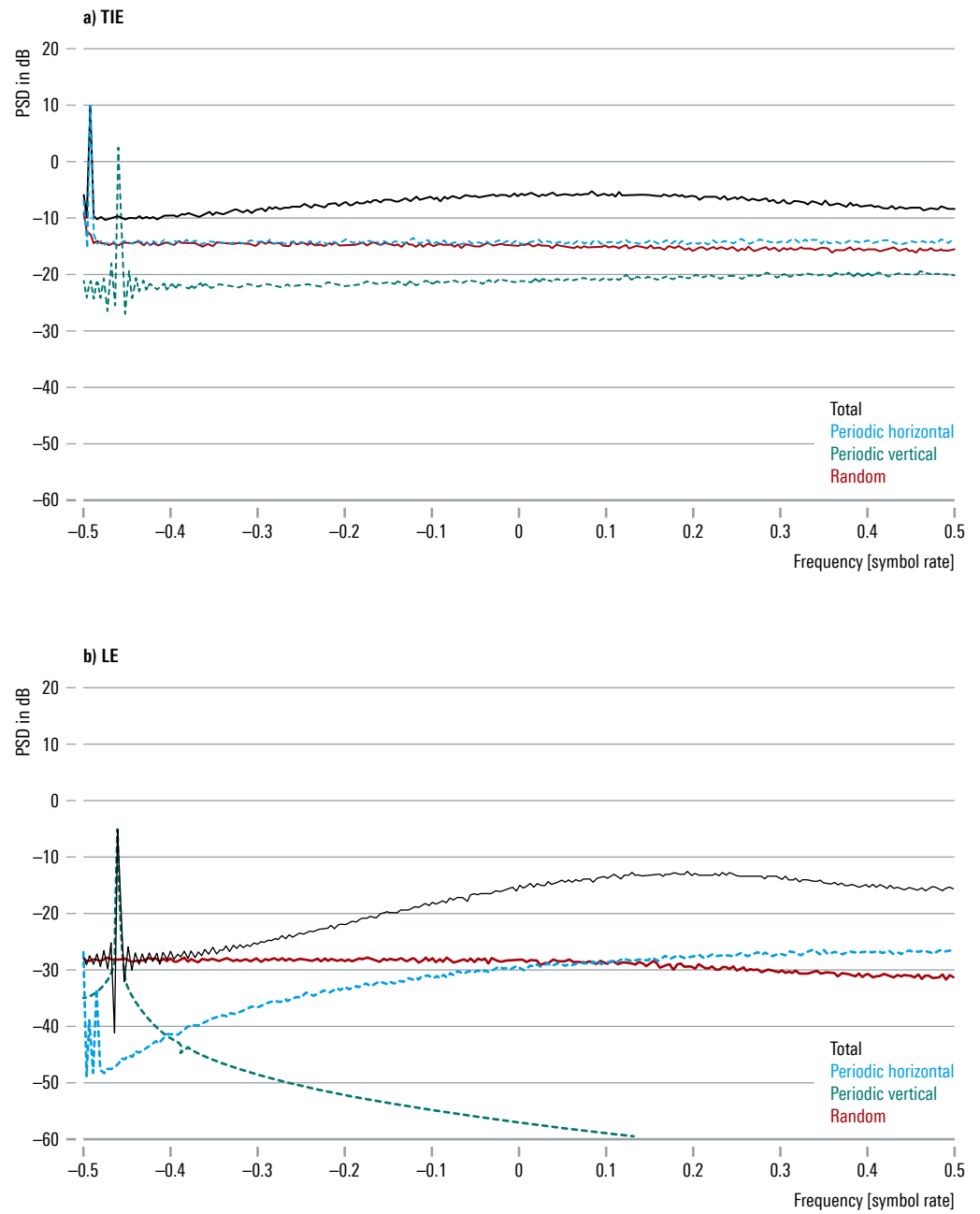
6.2 Signal length influence

It is crucial that the results produced by the framework are consistent and reliable. Therefore, we show that we can produce very similar results from different signal realizations with the same disturbances, even using small signal lengths.

We use scenario 2 from Table 1 with effective signal lengths varying from 1k to 2M (not accounting for the CDR lock time) symbols. For each length, we perform 100 simulations and analysis. Then, we evaluate the SD of various measurement results. Fig. 10 summarizes all these SDs vs. signal length and shows the respective linear least-squares fits in the logarithmic domains. We observe that, as expected, the measurements scale with $1/\sqrt{N_{smb}}$ with the number of (effective) symbols N_{smb}. For this scenario, the results are very precise even at a small length of 100k symbols. Thus for most applications, there is no need to go far beyond such a signal length. Moreover, this confirms that our framework uses a large portion of the information present in the input signal.

Fig. 10: SDs of the measured SDs vs. signal length
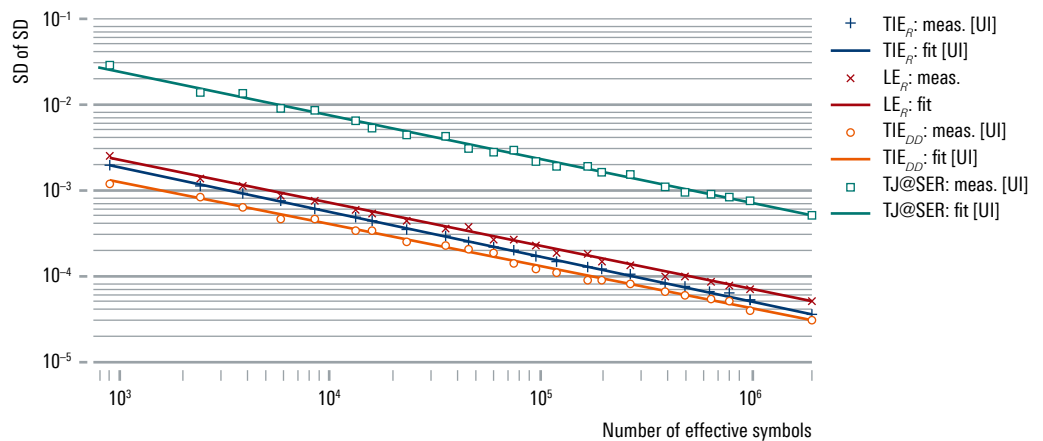
7 COMPARISON WITH COMPETING ALGORITHMS

Finally, we draw comparisons to other jitter analysis solutions. While it may seem natural to compare the results from our framework with those of other commercially available algorithms, care must be taken in the interpretation. We can feed the same signal, acquired with the same sampler, to a number of algorithms. However, none of the algorithms can be considered to be a reference or ground truth to compare against nor can the value of any added jitter or noise at the transmitter be regarded as a directly measurable quantity. Any jitter and noise analysis solution measures, e.g. the horizontal source disturbances transformed by the step responses and transmitted through the entire transmission system.

We attempt to draw comparisons with a commercial bit error rate tester (BERT) that performs BER measurements based on knowledge of the transmitted signal. However, there are differences in the input circuitry and the clock recovery of this device and that of the R&S®RTP with 8 GHz bandwidth that we use to acquire the signals. Thus, the results of the BERT still cannot be considered a reference for the remaining algorithms.

Ultimately, the only meaningful comparison is with respect to our own SER measurements, which are derived by assuming that the symbols are correctly decoded at the signal eyes' center. This has the drawback of requiring long signals and, at the same time, very low SERs at the eyes' center.

For the sake of completeness, we show some SER results derived by our framework as well as by commercially available algorithms. To this end, we define the three scenarios in Table 5 and configure the BERT to generate the appropriate signals. We use a second order PLL with a bandwidth factor of 1667 and a damping factor of 0.7 for these scenarios. The results are given in Fig. 11. The commercially available algorithms are spectral and tail fit algorithms from two vendors. The results with our framework are obtained with 1 Msample, while those of the state-of-the-art methods use 10 Msample. The SERs measured using the BERT are obtained with 10^{11} symbols.

In scenario 1 with a data rate of 1 Gbps, the calculation of the SER using our framework and all extrapolations of the SER are close to the measured SERs from the BERT and our framework [4]. However, the results from vendor 1 and vendor 2 slightly overestimate the SER at low and high sampling offsets; this is especially true at the sampling extremes for the vendor 2 results. Scenario 2 with a data rate of 3 Gbps is characterized by a higher amount of jitter. Here, the divergences between the results become more apparent. While the calculated SERs using our framework are able to closely match the measured SERs, the competing algorithms clearly overestimate the SER at sampling offsets around 0.25 and 0.75. Finally, scenario 3 with a data rate of 5 Gbps offers an even higher amount of jitter and the most obvious differences between the algorithms. Here, the commercially available algorithms provide results that are far off the measured SERs; this is especially true for the tail fit methods. In contrast, the calculated SERs from our framework follow the measured SERs much more closely.

Table 5: Settings for BERT scenarios

Property	Scenario 1	Scenario 2	Scenario 3
Data rate	1 Gbps	3 Gbps	5 Gbps
Sample rate	20 Gsample/s	20 Gsample/s	20 Gsample/s
Modulation	NRZ with ±175 mV differential signals	NRZ with ±175 mV differential signals	NRZ with ±175 mV differential signals
Symbol pattern	PRBS-23	PRBS-23	PRBS-23
Rate modulation	none	none	none
Cable length	2 m	2 m	2 m
Periodic horizontal disturbance $\epsilon_{h,P1}$	10 mUI pp at 86.12 MHz	15 mUI pp at 120 MHz	50 mUI pp at 120 MHz
Periodic horizontal disturbance $\epsilon_{h,P2}$	–	15 mUI pp at 35.5 MHz	15 mUI pp at 35.5 MHz
Random horizontal disturbance $\epsilon_{h,R}$	15 mUI RMS	45 mUI RMS	50 mUI RMS

[4] As in Section 6.1, note that the measured SERs diverge from the calculated/extrapolated SERs at low values, due to the low number of measured errors.

Fig. 11: SERs: proposed framework vs. competing algorithms

a) Scenario 1

b) Scenario 2

c) Scenario 3
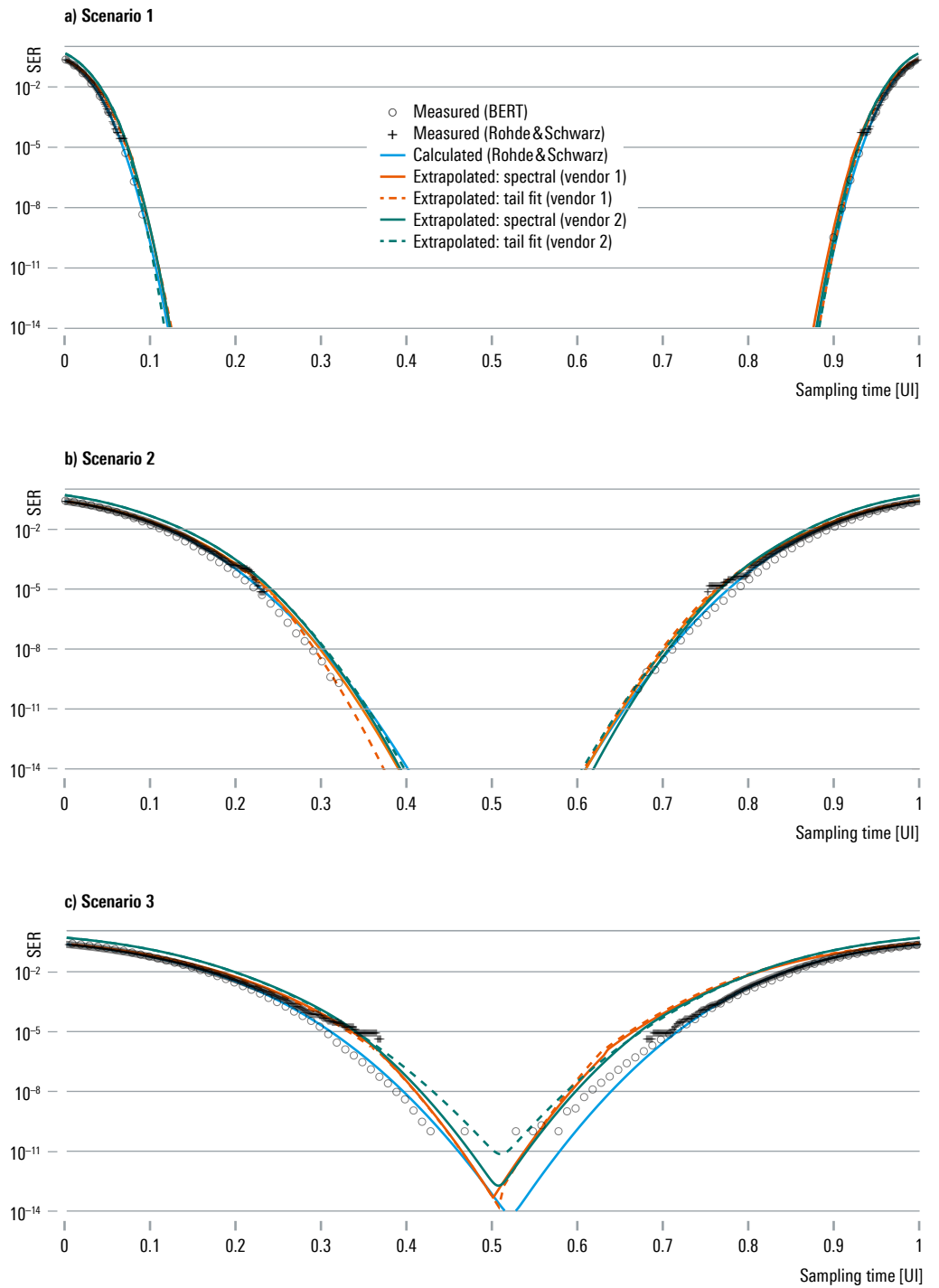
8 CONCLUSION

In this paper, we have introduced a joint jitter and noise analysis framework that is based on a signal model for PAM serial data transmission. In contrast to existing jitter analysis algorithms, we do not base our approach on TIEs only; instead we utilize all the information contained in the signal. We have demonstrated the potential of the proposed framework with exemplary measurement results as well as comparative studies with commercially available algorithms.

To summarize, there are several benefits to our approach. First, we provide additional, previously unavailable, measurements. Second, we require shorter signal lengths to achieve the same accuracy as state-of-the-art methods. Finally, our method does not rely on any specific symbol sequences.

Future work will focus on the consideration of OBU, the separation of horizontal and vertical components, and studies with higher order PAM.

9 REFERENCES

[1]   K. S. Oh and X. Yuan, "High-Speed Signaling: Jitter Modeling, Analysis, and Budgeting", Westford, MA, U.S.A.: Pearson Education, Inc., 2012.

[2]   M. P. Li, "Jitter, Noise, and Signal Integrity at High-Speed", Westford, MA, U.S.A.: Pearson Education, Inc., 2008.

[3]   M. P. Li, J. Wilstrup, R. Jessen, and D. Petrich, "A New Method for Jitter Decomposition Through Its Distribution Tail Fitting", International Test Conference, 1999.

[4]   M. P. Li and J. Wilstrup, "On the Accuracy of Jitter Separation From Bit Error Rate Function", International Test Conference, 2002.

[5]   "Jitter Analysis: The Dual-Dirac Model, RJ/DJ, and Q-Scale", Whitepaper: Keysight Technologies, U.S.A., Dec. 2017.

[6]   Q. Dou and J. A. Abraham, "Jitter Decomposition by Time Lag Correlation", Proceedings of the 7th International Symposium on Quality Electronic Design, 2006.

[7]   H. Pang, J. Zhu, and W. Huang, "Jitter Decomposition by Fast Fourier Transform and Time Lag Correlation", International Conference on Communications, Circuits and Systems, 2009.

[8]   K. Bidaj, J.-B. Begueret, and J. Deroo, "RJ/DJ Jitter Decomposition Technique for High Speed Links", 2016.

[9]   S. Erb and W. Pribyl, "Comparison of Jitter Decomposition Methods for BER Analysis of High-Speed Serial Links", 13th IEEE Symposium on Design and Diagnostics of Electronic Circuits and Systems, 2010.

[10]   C. Sui, D. G. Beetner, and T. Zhu, "A New Tail-Fit Method for Jitter Decomposition", IEEE International Symposium on Electromagnetic Compatibility, 2014.

[11]   C. Sui, S. Bai, T. Zhu, C. Cheng, and D. G. Beetner, "New Method to Characterize Deterministic Jitter and Crosstalk-Introduced Jitter From Measurements", IEEE Transactions on Electromagnetic Compatibility, 2014.

[12]   "Choosing the ISI Filter Size for EZJIT Plus Arbitrary Data Jitter Analysis", Application Note: Keysight Technologies Inc., 2017.

[13]   "Analyzing Jitter Using the EZJIT Plus Software", Application Note: Keysight Technologies Inc., 2017.

[14]   "Selecting RJ Bandwidth in EZJIT Plus Software", Application Note: Keysight Technologies Inc., 2017.

[15]   "Understanding and Characterizing Timing Jitter", Primer: Tektronix, 2012.

[16]   A. Blackman, "Understanding SDAII Jitter Calculation Methods", Technical Brief: LeCroy Corporation, 2012.

Rohde & Schwarz

The Rohde & Schwarz electronics group offers innovative solutions in the following business fields: test and measurement, broadcast and media, secure communications, cybersecurity, monitoring and network testing. Founded more than 80 years ago, the independent company which is headquartered in Munich, Germany, has an extensive sales and service network with locations in more than 70 countries.

www.rohde-schwarz.com

Rohde & Schwarz customer support

www.rohde-schwarz.com/support